



OPEN

A novel metamaterial-based antenna for on-chip applications for the 72.5–81 GHz frequency range

Karen N. Olan-Núñez & Roberto S. Murphy-Arteaga

In this paper we present a novel metamaterial-based antenna simulated using HFSS. The unit cell parameters were extracted using periodic boundary conditions and wave-port excitation. The metamaterial is magnetically coupled to the CPW line, the induced current in the hexagonal ring gives rise to a field perpendicular to the incident one. The antenna can be modeled by an LC circuit. This design achieves a significant impedance bandwidth of 8.47 GHz ($S_{11} = -10$ dB from 72.56 GHz to 81.03 GHz), and a minimum return loss of -40.79 dB at 76.89 GHz, which clearly indicates good impedance matching to 50Ω . The proposed antenna offers gains from 4.53 to 5.25 dBi, with radiation efficiencies better than 74%. Compactness, simple design layout, a novel design, and good radiation characteristics for this antenna are the main contributions of this work. The antenna can be built on top of a $300\ \mu\text{m}$ thick silicon wafer, for application on HR-SOI-CMOS technology. When compared to other antenna designs for the same frequency band, the proposed antenna achieves very good performance. This design is suitable for the reception stage of long-range automobile radar systems, due to its wide HPBW, as well as E-band applications, such as backhaul systems.

To meet the huge public demand for compact, wireless systems, antennas, beside the other necessary electronic circuitry, must be integrated on the same silicon chip, and thus research on on-chip antennas (AoC) has become a very important field of endeavor in recent years^{1–8}, just to mention a few.

On-chip antennas offer full monolithic integration of receivers and transmitters, with great repeatability, size reduction, low power consumption, and a reduction of external interconnections, such as bondwires or solder balls⁹. In fact, AoC have become a very dynamic field of endeavor, as the slew of recently published reports shows, spanning different techniques such as coupling and excitation techniques^{1–3}, isolation⁴, circuit design⁵, and the use of metamaterial and metasurface properties^{6–8}. Of the many applications that have been addressed by different research groups, one that falls in the 76–81 GHz is vehicular radar¹⁰. Vehicular radar systems are divided into two major areas, the signal processing and power supply unit; and the RF front-end, which contains the radar transceiver device and one or more TX and RX antennas¹¹. In fact, on-chip antennas are good candidates for these systems, mainly due to their compact size, low power consumption and the possibility to fully integrate the RF front-end. It is well known, however, that bulk silicon with typical conductivities in the range 1–10 S/m for standard CMOS processes leads to very poor antenna performance, e.g., typical antenna gains of -10 dBi, due to substrate losses¹².

Over the past few years, in order to improve the gain, directivity, and radiation efficiency, while overcoming the limitations of silicon substrates and maintaining reduced size, different types of metamaterials have been proposed, such as Artificial Magnetic Conductors, AMC; High Impedance Surfaces, HIS; Electromagnetic Band-Gap structures, EBG; Double Negative Materials, DNG; Zeroth Order Resonators, ZOR; and various types of metasurfaces^{13–20}. In other works, external resonators²¹, or lenses are used^{22,23}, micromachining is performed around and below the antenna²⁴, the doping profile around the antenna is tailored¹², its position is optimized²⁵, reflectors are employed²⁶, and high resistivity (HR) substrates are used^{27,28}.

Notwithstanding, the majority of on-chip antenna developments have been made on SOI (Silicon-On-Insulator) substrates with HR silicon, but achieving antenna gains in the range of -3 to 3 dBi. Such low gain values are appropriate for short-range communications, up to one meter; typical applications are the high-data rate

Electronics Department, Instituto Nacional de Astrofísica, Óptica y Electrónica (INAOE), 72840 Puebla, Mexico.
✉ email: rmurphy@ieee.org

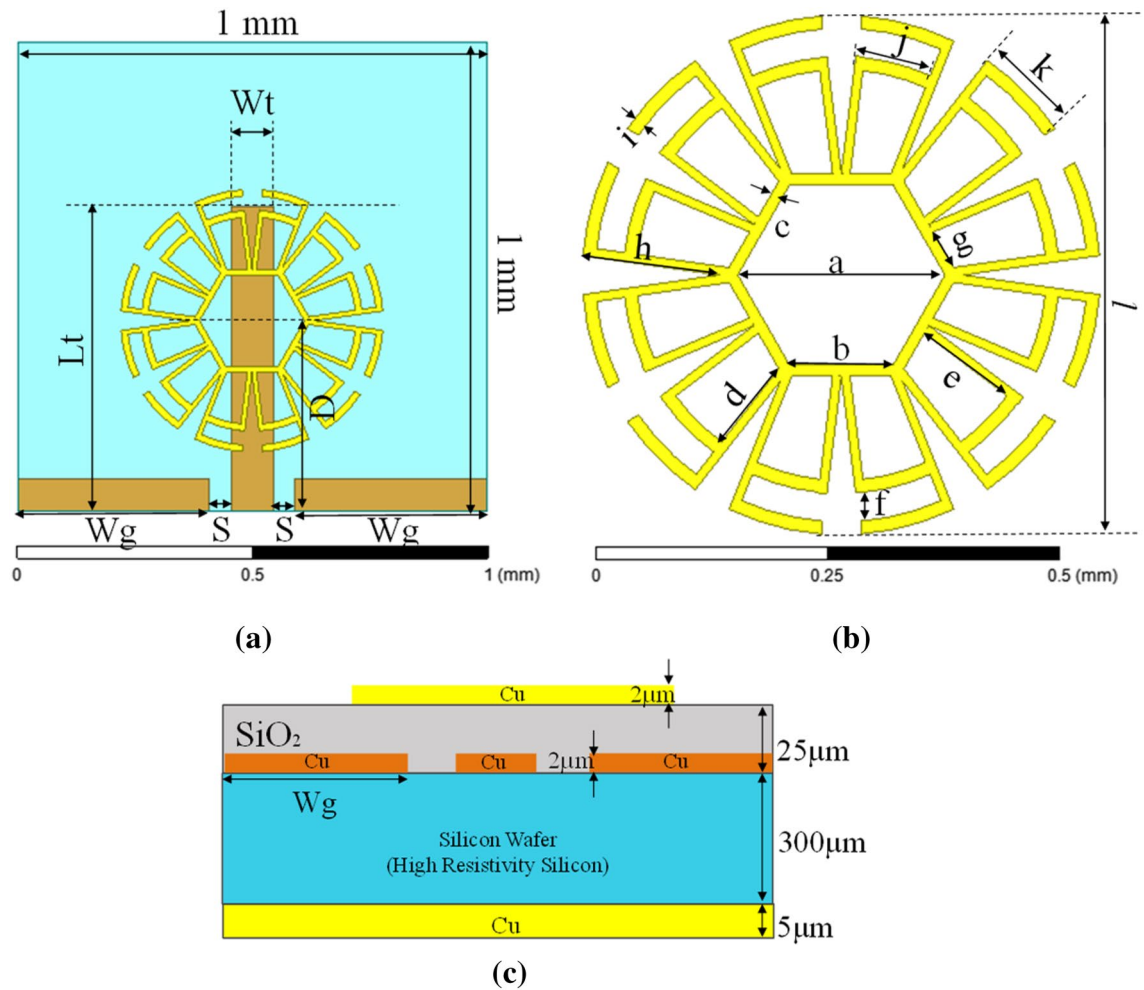


Figure 1. Top view of proposed antenna (a) flower-metamaterial antenna and feed line (CPW), (b) flower-metamaterial design and (c) cross-sectional view of proposed antenna.

transfer and synchronization between smart wireless devices (smart-phone, laptop, external hard drives) using a wireless USB-like connection¹².

In this paper, we present a novel antenna design based on metamaterial properties that operates in the millimeter wave regime. This design resembles the center of a flower with its petals, and thus we refer to it as a “Flower Metamaterial Antenna”. Unlike classic and traditional antennas, this one is based on a new metamaterial design to operate from 75 to 81 GHz on a HR silicon wafer, and it is excited by proximity with a coplanar waveguide (CPW), covering the spectrum for long-range automotive radars¹⁰, attaining higher gains to those obtained with SOI technology, and achieving good radiation efficiency.

Flower-metamaterial antenna design

The top view of the proposed antenna is shown in Fig. 1a,b. The CPW line used to excite the metamaterial is on a higher metal layer above a thin layer of silicon dioxide. To match the antenna’s input impedance, the width of the feed line (W_f) is calculated at 90 μm , and the gap between the feed and the ground line on either side (S) is fixed as 45 μm . This CPW feed is highly preferred over a microstrip line in on-chip antenna design since it exhibits lower losses when these lines are deposited directly on high resistivity silicon substrates and are less sensitive to bulk parameter variations such as changes in carrier concentration²⁷.

The design parameters for the proposed antenna were parametrically optimized using a full-wave simulator to obtain the desired results, which are listed in Table 1.

Figure 1c depicts a cross sectional view of the proposed structure. A 300 μm thick high resistivity silicon wafer ($\rho \geq 5 \text{ k}\Omega \text{ cm}$, $\tan \delta = 0.05$ and $\epsilon_r = 11.8$) was used as the substrate. The metamaterial is made of a 2 μm thick copper (Cu) layer. In between the substrate and the radiating structure, there is an insulating layer, namely SiO_2 ($\epsilon_r = 3.9$ and $\tan \delta = 0.001$) with a thickness of 25 μm , and the feed line (CPW) is placed 23 μm away from the radiating structure in a metal layer embedded in a SiO_2 layer. Besides, a 5 μm thick metal layer is used as a reflector on the back side.

| Parameter | Value (μm) | Parameter | Value (μm) | Parameter | Value (μm) |
|-----------|-------------------------|-----------|-------------------------|-----------|-------------------------|
| a | 224 | g | 44 | D | 400 |
| b | 112 | h | 140 | Lt | 650 |
| c | 10 | i | 14 | Wg | 410 |
| d | 99 | j | 78 | S | 45 |
| e | 110 | k | 100 | Wt | 90 |
| f | 29 | l | 560 | | |

Table 1. Design parameters.

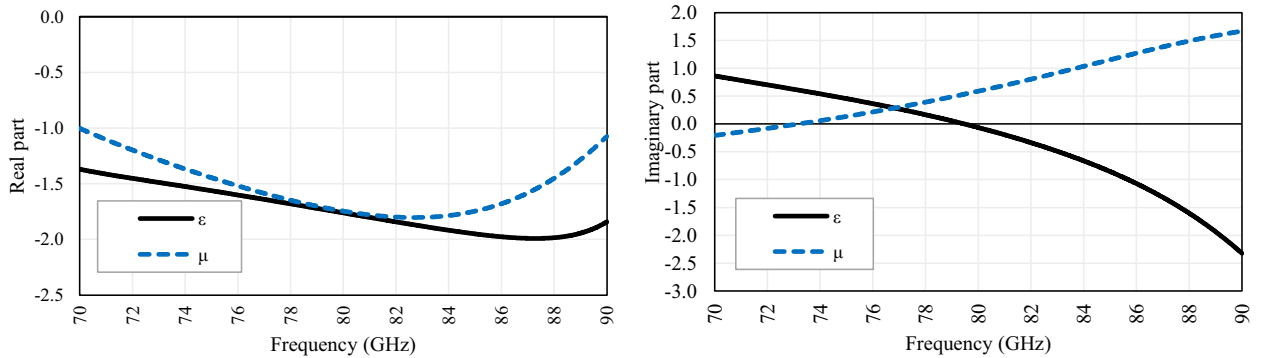


Figure 2. Complex permittivity (ϵ) and permeability (μ) of proposed flower geometry.

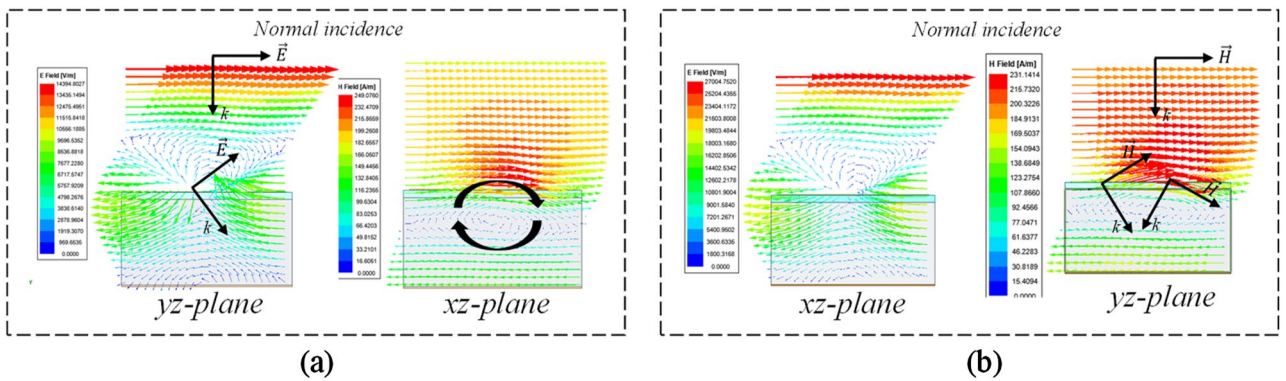


Figure 3. Electrical and magnetic fields for (a) TE_{00} mode, and (b) TM_{00} mode.

The Flower-Metamaterial structure was previously designed with the full-wave simulator without the feed line to ensure it behaves as a metamaterial structure. The design was performed following the methodology proposed in²⁹, and some details are presented in “Methods” section.

Figure 2 shows the real and imaginary parts of the permittivity and permeability of the design, demonstrating its metamaterial behavior (Left-Handed material) in the frequency band of interest, after a lengthy simulation process.

Moreover, when the unit cell is simulated using Floquet ports, the flower metamaterial presents an interesting behavior, which is shown in Fig. 3. From 72 to 81 GHz, the modes supported by the flower are TE_{00} and TM_{00} , and other modes (m, n ; different from zero) are attenuated (> 30 dB/mm). The flower unit cell changes de propagation direction, curves the direction of electric and magnetic fields, and partially eliminates the magnetic field concentration on the silicon wafer, confining it mostly on and above the flower.

The operation mechanism is as follows: when the CPW line is positioned below the metamaterial cell, the metamaterial cell is magnetically coupled to the CPW line. The magnetic field lines (of the CPW line) that pass through the hexagonal ring induce a current that gives rise to an electric field in a direction perpendicular to the incident wave. This magnetic coupling, the induced current, and the electric and magnetic fields are shown in Fig. 4.

The design of the proposed unit cell is a lengthy process and many variables play an important role. However, a brief design evolution is presented below with only 5 steps, comparing three important figures of merit considered during the design process.

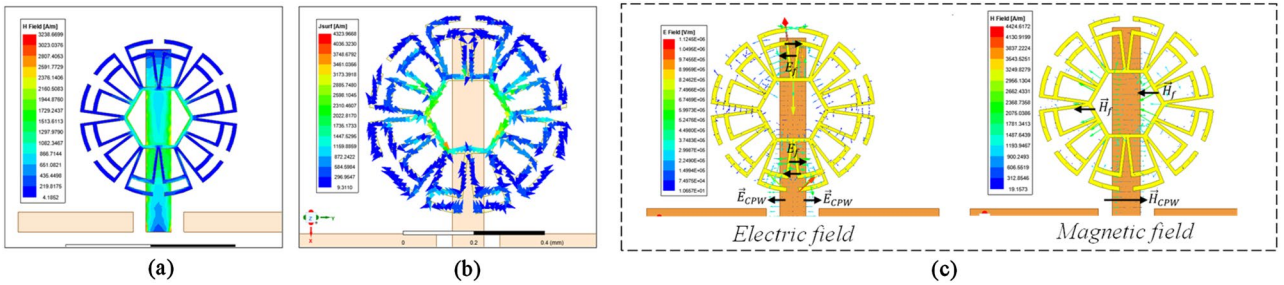


Figure 4. Operation mechanism: (a) magnetic coupling, (b) induced current, and (c) fields throughout the structure.

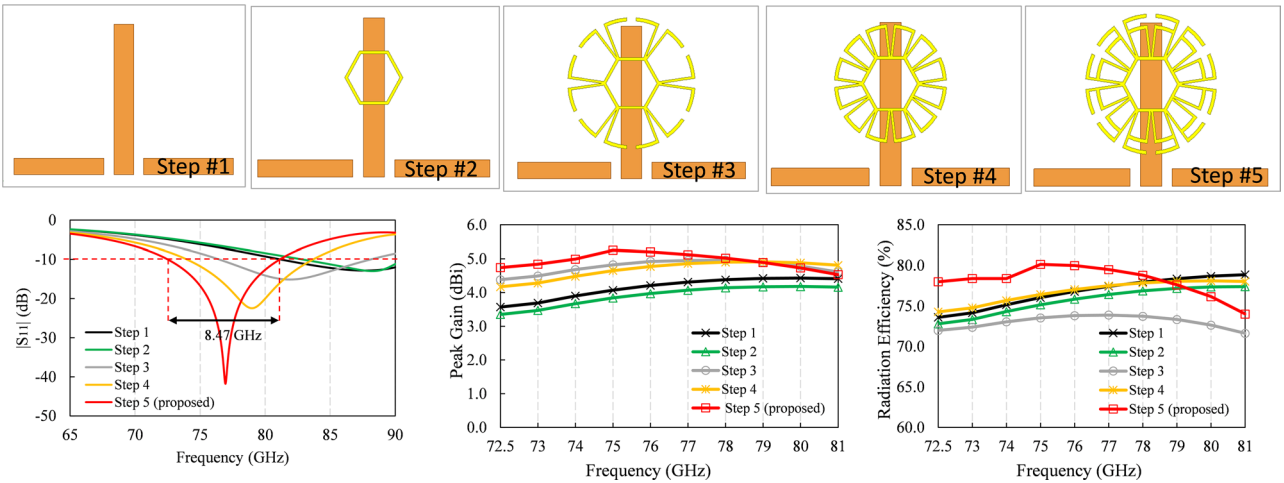


Figure 5. Brief design evolution of the proposed flower metamaterial-based antenna, and comparison of three of the figures of merit versus frequency.

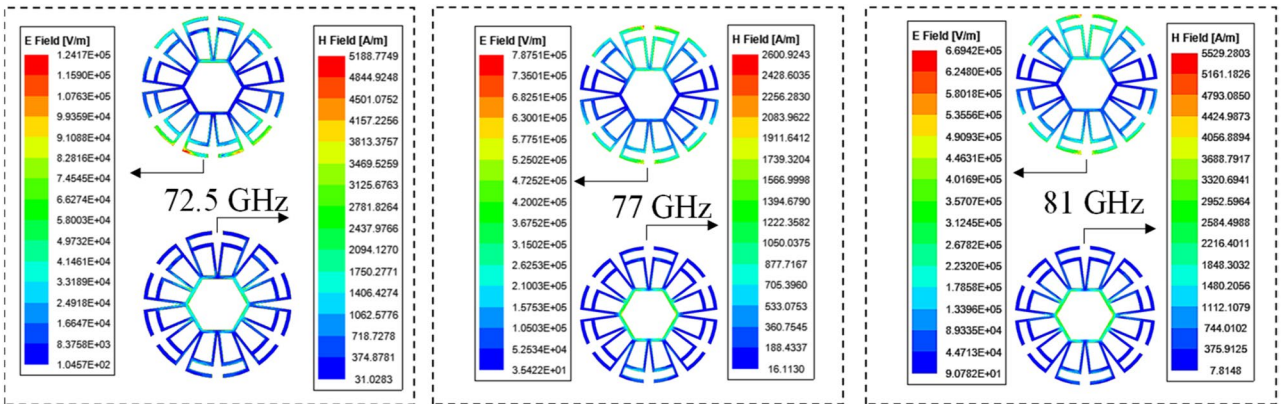


Figure 6. Electric (left side) and magnetic (right side) field magnitude at three frequency points: 72.5 GHz (lower), 77 GHz (central), and 81 GHz (higher).

Results

This section demonstrates that the proposed design has significant potential for on-chip radar systems, especially for the reception stage, due to its wide HPBW, high gain, small size and ease of fabrication. In the case of the transmitter stage, a moderate to high gain (better than 3 dBi) and a narrow beam are required, and some improvements to the design would be necessary to satisfy them.

Figure 5 shows the simulated return loss of the proposed novel flower metamaterial-based antenna and impedance bandwidth ($|S_{11}| \leq -10$ dB) of 8.47 GHz, from 72.56 GHz to 81.03 GHz, considering a reference impedance of 50 Ω . The electrical and magnetic planes (H-plane $\phi = 0^\circ$ and E-plane $\phi = 90^\circ$) radiation parameters (in magnitude) are presented in Fig. 6, which prove that the design covers the entire frequency band destined for long-range radars (76–81 GHz) and partially the E-band (71–86 GHz).

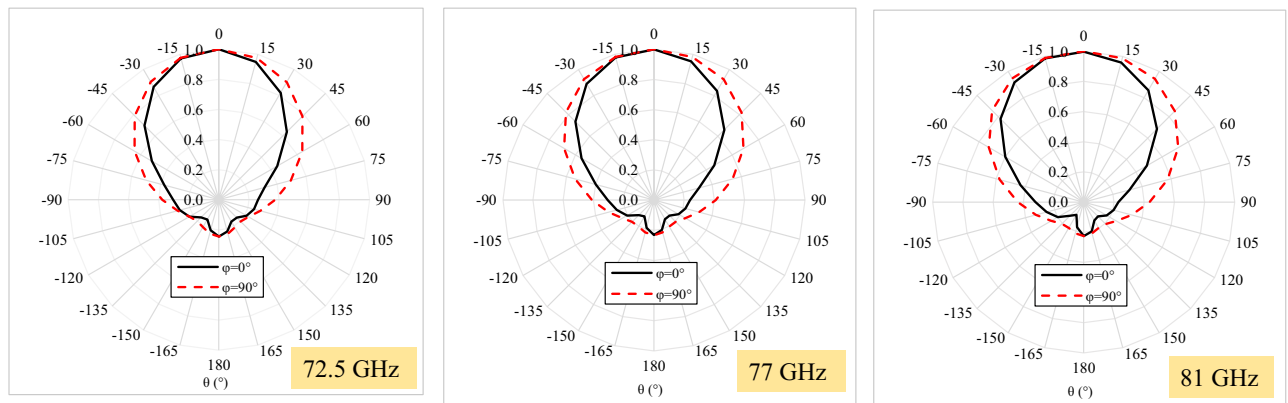


Figure 7. Normalized radiation patterns at three frequency points: 72.5 GHz (lower), 77 GHz (central), and 81 GHz (higher).

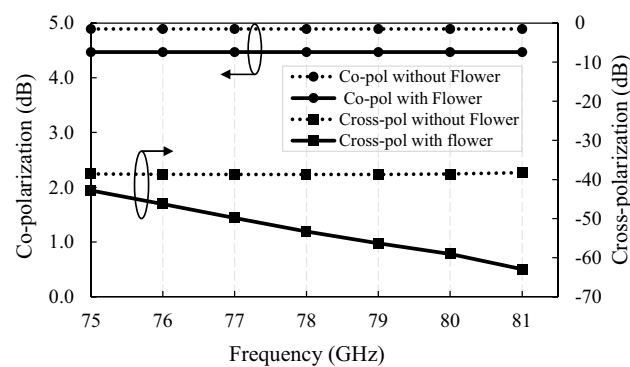


Figure 8. Comparison of cross-polarization and co-polarization versus frequency of the design with and without proposed flower metamaterial.

The 2D radiation patterns are shown in Fig. 7 for three frequency points (lower, central, and higher), remaining almost unchanged throughout the frequency range from 72.5 to 81 GHz, with only one beam and maintaining symmetry across the bandwidth. The front-back ratio is close to 19 dB, but a higher F/B ratio can be obtained by increasing the reflector plane size.

The comparison of co-polarization and cross-polarization, with and without flower metamaterial, is shown in Fig. 8. This design has cross-polarization values lower than -30 dB, and co-polarization greater than 4.5 dB, which guarantees that the waves are almost purely linearly polarized to the right, considering the values of axial ratio ($AR \rightarrow \infty$) and RHCP-LHCP gains, obtained from the full wave simulator.

Furthermore, the peak gains shown in Fig. 5 show that the proposed design improves gain by 32% at 72.5 GHz, 31.16% at 73 GHz, 27.94% at 74 GHz, 29% at 75 GHz, 23.51% at 76 GHz, 18.79% at 77 GHz, 14.61% at 78 GHz, 10.63% at 79 GHz, 6.8% at 80 GHz and 3.6% at 81 GHz. Likewise, the radiation efficiency is improved from 72.5 GHz to 78 GHz, and from 79 to 81 GHz it decreases slightly, but remains above 74%.

Furthermore, these curves show that the flower material acts as an LC circuit, due to the concentrations of electric and magnetic fields in the design. An equivalent circuit for the metamaterial-based antenna was derived, and it is shown in Fig. 9a. The lumped elements values of the model are: $L_L = 1.56pH$, $C_L = 2.53pF$, $L_1 = L_2 = 10.1fF$, $C_1 = 20fF$, $C_2 = C_3 = 66pF$, $C_4 = 0.1fF$, $C_{cpw} = 24.8fF$, $L_{cpw}/4 = 44.45pH$. The comparison between model and full-wave simulations is shown in Fig. 9b.

It is noteworthy that this is an original design, which has many advantages over other reported antennas for the same frequency range^{13,14,21,22,30,31}, whose characteristics are listed in Table 2.

It is important to consider that the designs on ceramic substrates attain a higher gain, since these materials have lower losses than a semiconductor substrate. These designs, however, occupy a very large area and have a narrower bandwidth than our design.

On the other hand²¹, has lower efficiency, occupies a larger area and volume, and is based on a quartz crystal. The design in¹³ has a higher bandwidth and does not occupy a large area, but the gain and coupling at the input are low. The antenna reported by¹⁴ is approximately 13 times larger than the one presented here, and achieves a gain of just 1.46 times that of the one obtained with the proposed design, in addition to presenting a 1 GHz bandwidth.

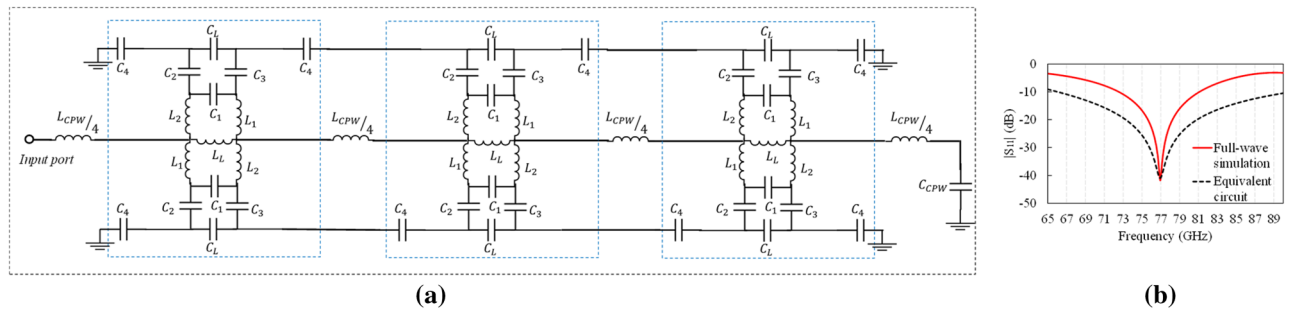


Figure 9. (a) Proposed equivalent circuit, and (b) comparison of equivalent circuit with full-wave simulation results.

| Parameter | References | | | | | | | | |
|-----------------------------|------------------------------------|----------------------------------|---|------------------------|---------------------------|-------------------------------|---------------------------------------|--------------------------|---------------------------------|
| | 21 | 22 | 13 | 14 | 30 | 31 | 8 | 4 | This work |
| Substrate and thickness (h) | SiGe | RO3003 and polyphenylene sulfide | Si h = 300 μm | Si h = 200 μm | RO3003 h = 127 μm | RO3010 4350B h = 598 μm | Two layers of polyimide h = 500 μm | Polyimide h = 125 μm | HR-Si h = 300 μm |
| Total area | ~ 3.5 mm ² | 594 mm ² | 1.95 mm ² | 12.96 mm ² | 442.26 mm ² | > 1500 mm ² | 36 mm ² | 270 mm ² | 1 mm ² |
| Design type | Two patches and two quartz glasses | Horn antenna, lens and prism | Monopole antenna, SRR and MIM capacitor | Patch antenna and CSRR | Planar micro-strip arrays | L-shaped slots array | CRLH-TL | SIW-loaded patch antenna | Novel flower-metamaterial |
| Reflection coefficient | - 20 dB | - 45 dB | - 10 dB | - 33.7 dB | < - 20 dB | < - 15 dB | < - 10 dB | - | - 40.79 dB |
| Bandwidth | N.A. | 7 GHz | 9 GHz | 1 GHz | 2 GHz | 7 GHz | 35 GHz | 10 GHz | 8.47 GHz |
| Gain | N.A. | 21.5 dBi | 1.6 dBi | 7.7 dBi | 23.3 dBi | 16 dBi | 8.15 dBi | Max. 12.2 dBi | 5.25 dBi |
| Directivity | N.A. | N.A. | N.A. | N.A. | N.A. | N.A. | - | - | 6.55 dBi |
| Radiation efficiency | 50% | N.A. | N.A. | ~ 70% | N.A. | N.A. | 65.71% | Max. 86% | 80.1% |
| HPBW | N.A. | 22° | 25° | N.A. | 12.2° | 9.1° | - | - | 126° (φ = 0°) 163° (φ = 90°) |
| Design frequency | 77 GHz | 77 GHz | 77–87 GHz | 77 GHz | 77 GHz | 79 GHz | 0.350–0.385 THz | 0.19–0.20 THz | 72.5–81 GHz |

Table 2. Comparison with related works. *N.A.* not available, *SRR* split ring resonator, *CSRR* composite split ring resonator, *CRLH-TL* composite right-left handed transmission line, *SIW* substrate integrated waveguide.

Finally, the half power beam width in all the cases is lower than the one obtained in our design, which means that those designs have very fine beams, which are appropriate for the transmission stage, but not for Rx antennas, which require a large field of view³².

Additionally, when the proposed design is compared with designs working at THz range^{4,8}, this design has lower gain, since both designs^{4,8} use polyimide as substrate; therefore it is to be expected that the gains will be higher, because the substrate has a lower loss coefficient. Compared with⁸ the proposed novel design has higher efficiency, and is 36 times smaller, and compared with⁴, our design is 270 times smaller, even when the operating frequency of our design is lower.

Discussion

Herein we have presented a novel flower-metamaterial antenna designed to work from 72.5 to 81 GHz. This antenna design, on a HR-Silicon wafer, has medium to high gain, acceptable directivity, good radiation efficiency, wide bandwidth, and compact size, which is ideal for on-chip automobile radar applications, particularly for the reception stage, considering its wide HPBW.

The radiation pattern shows only one beam from 72.5 to 81 GHz. A higher F/B ratio can be obtained by increasing the reflector plane size, and the polarization is almost purely linear, due to good values of cross-polarization and co-polarization in all the range.

The suggested fabrication process for prototyping of the proposed design is as follows: the ground plane, flower metamaterial, and feed line can be of 1–2 μm of copper or aluminum. The thick layer of silicon dioxide can be obtained from wet thermal oxidation process, but also can be replaced with other material, such as polyamide or polyimide, and some dimensions should be adjusted to ensure the impedance bandwidth from 72.5 to 81 GHz.

The new proposed antenna based on the so-called “flower metamaterials” can be integrated into a HR-SOI-CMOS process, in the last layer of the BEOL, that is, because a separation between the excitation line and metamaterial of 23 μm is required, when SiO₂ is used between both metal layers.

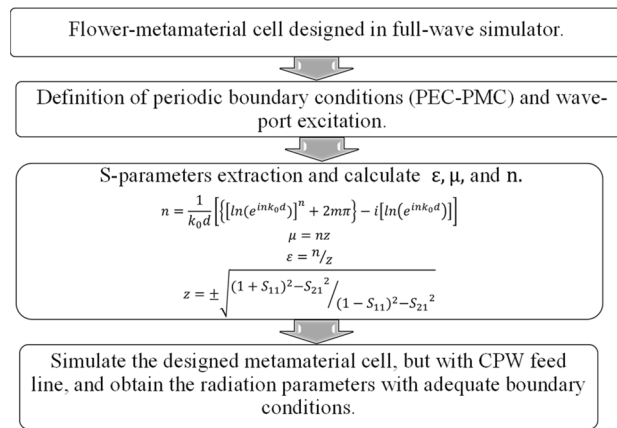


Figure 10. Methodology for design and extraction of parameters of unit cell metamaterial.

Methods

All the full-wave simulations were performed using Ansys electromagnetics suite 2021/R1 (High Frequency Structure Simulator, HFSS) (<https://www.ansys.com/products/electronics/ansys-hfss>).

For the design and extraction of the parameters of the metamaterial unit cell, the process presented in Fig. 10 was followed. It is an iterative process. Additional simulations were performed with Floquet ports and master–slave conditions to calculate the modes that the flower metamaterial supports, as well as the fields, which are presented in Fig. 3.

For the radiation parameters Ansys is also used, with a lumped port for the excitation with input impedance of 50 Ω and radiation box with dimensions better than λ_0 (at 80 GHz). Multiple solution frequencies are used in the simulation to guarantee accuracy across the frequency sweep.

The equivalent circuit was modeled with Advanced Design System (ADS). The proposed equivalent circuit is based on transmission line theory. The three stage shown in Fig. 9a (in blue boxes) represent the flower divided in three parts; C_4 represents the capacitance between the petals of the flower shape; L_L and C_L are the principal elements of this equivalent circuit, both represent the electromagnetic fields at resonant frequency; and $L_{cpw}/4$ and C_{cpw} are the lumped elements of the CPW line. The term $L_{cpw}/4$ represents the inductance when the flower is magnetically coupled to the transmission line.

Conclusions

Herein we have presented a novel flower-metamaterial antenna working from 72.5 to 81 GHz. This antenna design over HR-Silicon wafer has medium–high gain (better than 4.5 dBi), good radiation efficiency (higher than 74%), wide impedance bandwidth (8.47 GHz), and compact size (1 mm²). Moreover, here we present an equivalent circuit of the novel flower metamaterial-based antenna. The proposed design is suitable for applications of E-band, such as backhaul systems, and automobile radar systems.

Received: 8 September 2021; Accepted: 12 January 2022

Published online: 01 February 2022

References

- Alibakhshikenari, M. *et al.* High-gain on-chip antenna design on silicon layer with aperture excitation for terahertz applications. *IEEE Antennas Wirel. Propag. Lett.* **19**, 1576–1580. <https://doi.org/10.1109/LAWP.2020.3010865> (2020).
- Alibakhshikenari, M., Virdee, B. S., Althuwayb, A. A., Mariyanayagam, D. F. & Limiti, E. Compact and low-profile on-chip antenna using underside electromagnetic coupling mechanism for terahertz front-end transceivers. *Electronics* **10**, 1–7. <https://doi.org/10.3390/electronics10111264> (2021).
- Fan, Y., Xie, S., Luo, Y. & Ma, K. Gain and radiation efficiency enhance terahertz on-chip antenna based on 0.13-mm SiGe BiCMOS. In *Proceedings of the 14th UK-Europe-China Workshop on Millimeter-Waves and Terahertz Technologies (UCMMT)*. 1–3, <https://doi.org/10.1109/UCMMT53364.2021.9569947> (2021).
- Alibakhshikenari, M. *et al.* High-isolation antenna array using SIW and realized with a graphene layer for sub-terahertz wireless applications. *Sci. Rep.* **11**, 1–14. <https://doi.org/10.1038/s41598-021-87712-y> (2021).
- Mustacchio, C., Boccia, L., Arneri, E. & Amendola, G. A gain leveling technique for on-chip antennas based on split-ring resonators. *IEEE Access*. **9**, 90750–90756. <https://doi.org/10.1109/ACCESS.2021.3091777> (2021).
- Alibakhshikenari, M. *et al.* Study of on-chip antenna design based on metamaterial-inspired and substrate-integrated waveguide properties for millimeter-wave and THz integrated-circuit applications. *J. Infrared Millim. Terahertz Waves*. **42**, 17–28. <https://doi.org/10.1007/s10762-020-00753-8> (2020).
- Althuwayb, A. A. *et al.* Antenna on-chip (AoC) design using metasurface and SIW technologies for THz wireless applications. *Electronics* **10**, 1–8. <https://doi.org/10.3390/electronics10091120> (2021).
- Alibakhshikenari, M. *et al.* High-gain metasurface in polyimide on-chip antenna based on CRLH-TL for sub-terahertz integrated circuits. *Sci. Rep.* **10**, 1–9 (2020).
- Chen, Z. N., Liu, D., Nakano, H., Qing, X. & Zwick, T. *Handbook of Antenna Technologies 2445–2498* (Springer Singapore, 2016).
- Federal Communications Commission. Radar services in the 76–81 GHz band Report and Order – ET Docket. *FCC-CIRC1707-07*. 15–26, <https://docs.fcc.gov/public/attachments/DOC-345476A1.pdf>. (2017).

11. Rao, S. MIMO radar. *Texas Instruments Application Report SWRA554A*. https://www.ti.com/lit/an/swra554a/swra554a.pdf?ts=1620165925990&ref_url=https%253A%252F%252Fwww.google.com%252F (2018).
12. Dussopt, L. Integrated antennas and antenna arrays for millimetre-wave high data-rate communications. In *Proceedings of the 2011 Loughborough Antennas & Propagation Conference*. 1–5, <https://doi.org/10.1109/LAPC.2011.6114000> (2011).
13. Mustacchio, C., Boccia, L., Arneri, E. & Amendola, G. Gain enhancement technique for on-chip monopole antenna. In *Proceedings of the 50th European Microwave Conference (EuMC)*. 650–653, <https://doi.org/10.23919/EuMC48046.2021.9338160> (2021).
14. Li, Q., Li, W., Ren, B., Zhang, L. & Zhang, B. A silicon-based on-chip antenna operating at 77GHz. In *2019 Photonics & Electromagnetics Research Symposium-Fall (PIERS-Fall)*. 2848–2852, <https://doi.org/10.1109/PIERS-Fall48861.2019.9021682> (2019).
15. Dong, Y. & Itoh, T. Metamaterial-based antennas. *Proc. IEEE* **100**, 2271–2285 (2012).
16. Manh, C. T., Ouslimani, H. H., Guida, G., Priou, A., Teillet, H. & Daden, J. Y. Metamaterial structures for compact millimeter wave antenna applications. In *Proceedings of Progress in Electromagnetics Research Symposium*. 1306–1312 (2008).
17. Wasel, H. & Guoping, Z. Enhancing 5G patch array antenna gain using DNG metamaterial. *Int. J. Energy Eng.* **8**, 93–96. <https://doi.org/10.5923/j.ijee.20180804.02> (2018).
18. Devapriya, A. T. & Robinson, S. Investigation on metamaterial antenna for terahertz applications. *J. Microwav. Optoelectron. Electromagn. Appl.* **18**, 377–389. <https://doi.org/10.1590/2179-10742019v18i31577> (2019).
19. Badawe, M. E., Almoneef, T. S. & Ramahi, O. M. A true metasurface antenna. *Sci. Rep.* **6**, 1–8. <https://doi.org/10.1038/srep19268> (2016).
20. Sajin, G. I. & Mocanu, I. A. “Metamaterial CRLH antennas on silicon substrate for millimeter-wave integrated circuits. *Int. J. Antennas Propag.* **1–9**, 2012. <https://doi.org/10.1155/2012/593498> (2012).
21. Hasch, J., Wostradowski, U., Gaier, S. & Hansen, T. 77 GHz radar transceiver with dual integrated antenna elements. In *German Microwave Conference Digest of Papers*. 280–283, <https://ieeexplore.ieee.org/document/5498268> (2010).
22. Nagaishi, H., Kuriyama, A., Kuroda, H. & Kitayama, A. Horn and prism antenna for dual range and dual FOV automotive radar using 77-GHz band. In *Proceedings of the 18th International Symposium on Antenna Technology and Applied Electromagnetics (ANTEM)*. 1–2, <https://doi.org/10.1109/ANTEM.2018.8572918> (2018).
23. Cheema, H. M. & Shamim, A. The last barrier: On-chip antennas. *IEEE Microw. Mag.* **14**, 79–91. <https://doi.org/10.1109/MMM.2012.2226542> (2013).
24. Infineon Technologies AG., Meyer, T., Hartner, W. & Wojnowski, M. On-chip antennas for semiconductor devices and related manufacturing methods. *United States Patent No. US 2019/0221531 A1*. <https://patents.google.com/patent/US20190221531A1/en> (2019).
25. Ng, H. J., Wang, R. & Kissinger, D. On-chip antennas in SiGe BiCMOS technology: challenges, state of the art and future directions. In *Proceedings of the 2018 Asia-Pacific Microwave Conference (APMC)*. 621–623, <https://doi.org/10.23919/APMC.2018.8617626> (2018).
26. Hedayati, M. K. *et al.* Challenges in on-chip antenna design and integration with RF receiver front-end circuitry in nanoscale CMOS for 5G communication systems. *IEEE Access.* **7**, 43190–43204. <https://doi.org/10.1109/ACCESS.2019.2905861> (2019).
27. Lederer, D. & Raskin, J. P. Substrate loss mechanisms for microstrip and CPW transmission lines on lossy silicon wafers. In *Proceedings of the 2002 IEEE MTT-S International Microwave Symposium, Seattle*. 685–688, <https://doi.org/10.1109/MWSYM.2002.1011714> (2002).
28. Singh, K., Nirmal, A. V. & Sharma, S. V. Study the loss of microstrip on silicon. *Microwaves and RF*. <https://www.mwrf.com/technologies/components/article/21848246/study-the-loss-of-microstrip-on-silicon> (2017).
29. Numan, A. B. & Sharawi, M. S. Extraction of material parameters for metamaterials using a full-wave simulator [education column]. *IEEE Antennas Propag. Mag.* **55**(5), 202–211. <https://doi.org/10.1109/MAP.2013.6735515> (2013).
30. Dong, J. & Zhang, L. Reconfigurable antenna for automotive radar system. In *Proceedings of the 2019 IEEE International Symposium on Antennas and Propagation and USNC-URSI Radio Science Meeting*. 1155–1156, <https://doi.org/10.1109/APUSNCURSINRSM.2019.8888847> (2019).
31. Xie, J., Wu, Q., Yu, C., Wang, H. & Hong, W. Wideband SIW cavity-backed slot array antenna with flat gain characteristics for 79 GHz automotive radar. In *Proceedings of the 13th European Conference on Antennas and Propagation (EuCAP)*. 1–4 <https://ieeexplore.ieee.org/document/8739815> (2019).
32. Sickinger, F., Weissbrodt, E. & Vossiek, M. 76–81 GHz LTCC antenna for an automotive miniature radar frontend. *Int. J. Microw. Wirel. Technol.* **10**, 729–736. <https://doi.org/10.1017/S1759078718000855> (2018).

Acknowledgements

The authors would like to express their gratitude towards Mexican National Council for Science and Technology (CONACyT) by the financial support under Grant 852217 and Grant 285199.

Author contributions

K.N. conceived the idea, designed the structure, and wrote the principal ideas. R.M revised the manuscript, contributed some ideas, and supervised the work.

Funding

This work was supported in part by the Mexican National Council for Science and Technology (CONACyT) under Grant 285199 and Grant 852217.

Competing interests

The authors declare no competing interests.

Additional information

Correspondence and requests for materials should be addressed to R.S.M.-A.

Reprints and permissions information is available at www.nature.com/reprints.

Publisher's note Springer Nature remains neutral with regard to jurisdictional claims in published maps and institutional affiliations.



Open Access This article is licensed under a Creative Commons Attribution 4.0 International License, which permits use, sharing, adaptation, distribution and reproduction in any medium or format, as long as you give appropriate credit to the original author(s) and the source, provide a link to the Creative Commons licence, and indicate if changes were made. The images or other third party material in this article are included in the article's Creative Commons licence, unless indicated otherwise in a credit line to the material. If material is not included in the article's Creative Commons licence and your intended use is not permitted by statutory regulation or exceeds the permitted use, you will need to obtain permission directly from the copyright holder. To view a copy of this licence, visit <http://creativecommons.org/licenses/by/4.0/>.

© The Author(s) 2022